UC Irvine
UC Irvine Previously Published Works

Title
Spectrally-resolved imaging of dynamic turbid media

Permalink
https://escholarship.org/uc/item/1fk4v3c7

ISBN
9780819484291

Authors
Hagen, Nathan
Bedard, Noah
Mazhar, Amaan
et al.

Publication Date
2011-02-10

DOI
10.1117/12.875406

Copyright Information

Peer reviewed

Spectrally-resolved imaging of dynamic turbid media

Nathan Hagen[a], Noah Bedard[a], Amaan Mazhar[b], Soren Konecky[b], Bruce J. Tromberg[b], and
Tomasz S. Tkaczyk[a]

[a]Rice University, Bioengineering Department, Houston TX 77005
[b]University of California, Irvine, Department of Biomedical Engineering, Irvine CA 92612

ABSTRACT

We present a rapid, noncontact imaging technique which can obtain the spectrally- and spatially-resolved scattering and absorption coefficients of a turbid medium. The measurement involves combining a spatially modulated illumination pattern with a snapshot imaging spectrometer for measurement. After capture of an (x, y, λ) datacube, an image demodulation scheme is applied in post-processing to obtain the spatial maps of diffuse reflectance, absorption coefficient, and reduced scattering coefficient. The resulting system is used to dynamic maps (in 1 s intervals) of the brain's intrinsic optical signal.

1. INTRODUCTION

Functional imaging of optically diffuse media such as biological tissue can be difficult due to the nonlinear coupling between the scattering and absorption coefficients caused by their volumetric interaction inside the medium. In the visible and near-infrared regions, spectrally-resolved measurements of these coefficients for biological tissue provide a rapid noncontact means of mapping chromophore concentration, providing a measure of hemodynamics as well as the dynamic changes of any other chromophores. For brain imaging, this can be used to localize specific neural processes and to determine functional organization. This type of widefield spectral imaging system can also be used to dynamically map drug delivery within the body, either transcutaneously via chromophore distribution within subcutaneous vasculature, or directly within tissues.

Spatial frequency domain imaging (SFDI) is a technique for separating the absorption and scattering coefficients in turbid media which allows for wide-field optical property mapping and tomographic imaging. While SFDI has been used together with spectrally-resolved measurement in previous experiments, we show experiments in which it is used in combination with a snapshot imaging spectrometer for maximum optical throughput and time-resolution of dynamic data. After introducing SFDI and the image mapping spectrometer used in the experiments, we show validation data on tissue phantoms and present data showing the hemodynamic response of the brain to external stimulus. Whereas previous imaging spectrometry — based on liquid-crystal tunable filters — required 50 s to complete a 34-wavelength SFDI measurement, the IMS-based system can complete the same measurement in 1 s and provides 46 wavelengths.

2. SPATIAL FREQUENCY DOMAIN IMAGING

Spatial frequency domain imaging (SFDI) is a technique of illuminating a diffuse sample with discrete spatial frequencies and measuring the modulation contrast of the remitted light. This takes advantage of the principle that when sinusoidally modulated or structured light illuminates tissue, higher spatial frequencies attenuate more rapidly with depth than lower frequencies. Thus, if one looks for the contrast of reflected spatial fringes, one finds that lower spatial frequencies are sensitive to deeper regions, while higher spatial frequencies are sensitive to surface regions.[1,2] This property of differential depth sensitivity between DC and AC illumination also allows the separation of absorption and scattering coefficients within the sample. Since the DC frequency preferentially selects photons with the longest path length, it tends to be the most attenuated by absorption. The nonzero frequencies select shorter paths and so are relatively more sensitive to scattering. The ability of SFDI to quantitatively image both absorption and scattering[2] has been demonstrated by imaging stroke in the rat cerebral cortex,[3] cortical spreading depression,[4] layered structures in skin,[5] and hemodynamics in the human arm.[6]

The SFDI method works well for narrow band (quasi-monochromatic) illumination. When the illumination is broadband, and the sample contains spectrally-dependent scattering and absorption features, separation of the two optical properties requires spectrally resolved imaging. Since the method is camera-based and does not involve scanning, it allows one to quickly generate high resolution images over a large field of view.

For SFDI, the tissue is illuminated with a spatial pattern of the form

$$S = \frac{S_0}{2}\Big[1 + \cos(2\pi f_x + \phi)\Big] \,,$$

where S_0 is the mean illumination intensity, f_x the spatial frequency, and ϕ the spatial phase, respectively. The diffusely reflected intensity I for illumination pattern phase ϕ is given by

$$I = \frac{I_{\text{DC}}}{2}\big[1 + M_{\text{AC}}\,\cos(2\pi f_x + \phi)\big] \,,$$

a sum of DC (spatially uniform) and AC (spatially modulated) components. Here $M_{\text{AC}}(x, f_x)$ represents the modulation contrast — the amplitude of the reflected photon density "standing wave" at frequency f_x and position x.

To obtain $M_{\text{AC}}(x, f_x)$, we use a simple time domain amplitude demodulation method.[7] This involves illuminating the sample with a fixed spatial frequency sinusoid pattern but with three different phase offsets $\phi_1 = 0$, $\phi_2 = 2\pi/3$ and $\phi_3 = 4\pi/3$ radians. $M_{\text{AC}}(x, f_x)$ can then be calculated algebraically at each spatial location x by

$$M_{\text{AC}}(x, f_x) = \frac{\sqrt{2}}{3}\Big[(I_1 - I_2)^2 + (I_2 - I_3)^2 + (I_3 - I_1)^2\Big]^{1/2} \,.$$

The spatially-varying DC amplitude $I_{\text{DC}}(x)$ can be calculated at any frequency of illumination using $I_{\text{DC}}(x, f_x) = (I_1 + I_2 + I_3)/3$. Finally, measurement of a reference turbid phantom of known optical properties allows model-based calibration for the source intensity S_0, and therefore conversion of M_{DC} to calibrated diffuse reflectance R_{DC}:

$$R_{\text{DC}} = \frac{I_{\text{DC}}(\text{sample})}{I_{\text{DC}}(\text{reference})} \times R_{\text{DC}}(\text{reference}) \,.$$

This calibration step also corrects for any unwanted spatial variation in the illumination intensity $S_0(x, y)$ and for spatially-varying detection sensitivity (such as due to vignetting in the imaging lenses).

Once we have obtained R_{DC} and M_{AC}, we can calculate tissue optical properties by fitting to a lookup table created with a forward Monte Carlo model[2] simulating the two spatial frequencies used for the experiment, in this case $0\,\text{mm}^{-1}$ and $0.12\,\text{mm}^{-1}$. This lookup table search is performed independently for each voxel of the sample's (x, y, λ) datacube, producing a datacube for both the absorption coefficient μ_{a} and the reduced scattering coefficient μ_{s}'. Figure 1 shows the optical layout for the experiments. A commercial projector is used to illuminate the sample with white light distributed as a spatial sinusoidal pattern. The reflected light is imaged by an image mapping spectrometer (IMS) which obtains an (x, y, λ) datacube for each integration period. The SFDI algorithms then map the set of four measured datacubes to two optical property datacubes.

3. IMAGE MAPPING SPECTROMETRY

The operating principle of the image mapping spectrometer (IMS) system[8–10] is illustrated in Fig. 2. The sample is imaged onto at a custom-made microfaceted mirror called the "image mapper". The mapper is composed of a series of mirror facets, each with its own 3D tilt angle designed to direct the reflected light into one of an array of spectrometers, all of which are coupled to the same monolithic detector array. A mirror facet thus acts as an effective slit for its corresponding spectrometer, and the facets segment the image into set of narrow strips, which are then re-assembled after detection into an (x, y, λ) datacube by a re-mapping algorithm. In order to keep the system compact, the array of spectrometers is fabricated using arrays of miniature prisms and lenses which are each mounted onto a shared planar optomechanical support.

The resulting raw image is thus a one-to-one map of the datacube voxels onto a planar detector array, allowing for direct detection of the intensity from each voxel. From the raw data, we then remap the pixels
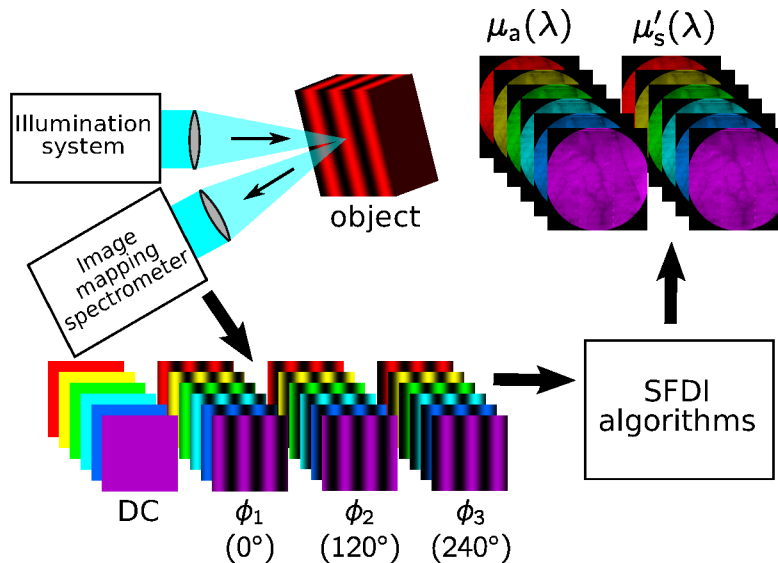
Figure 1: The experiments involve illuminating the sample with broadband light in a sequence of 4 different spatial patterns. The first pattern is unmodulated (DC), while the following three are each modulated by the same spatial frequency but are shifted in phase from one another by 120°. The remitted light is captured by the IMS imaging spectrometer, so that then SFDI algorithms produce two cubes of data: $\mu_a(x, y, \lambda)$ and $\mu'_s(x, y, \lambda)$.

onto the object voxels using the system calibration data, so that there is no need for solving an inverse problem via a reconstruction algorithm. This avoids the problem of image artifacts and noise amplification common to computational sensing methods. The dimensions of the data cube obtainable with the IMS depend on the size of the detector array — the total number of voxels cannot exceed the total number of pixels on the camera. In practice, we find that the IMS system can usefully map about 90% of the detector pixels, with the remaining 10% needed to provide margins between the subimages (see Fig. 2). When designing an IMS system for a given detector array, one can always increase the spatial sampling at the expense of spectral sampling, and vice-versa, as long as their product remains the same.

4. EXPERIMENTS: VALIDATION WITH PHANTOMS

In order to validate the SFDI algorithms and overall system, we constructed phantoms made of polydimethyl-siloxane (PDMS, *i.e.* "silicone"), in which two cylindrical regions within the sample are filled with a diluted intralipid solution and a colored dye — either Janus Green or Nigrosin Blue. Varying the amount of intralipid and dye within each well allows us to independently change the absorption coefficient μ_a and reduced scattering coefficient μ_s within the wells. The silicone phantom itself is always kept within the field of view in order to maintain a constant reference of $\mu_a \approx 0.02$, $\mu'_s \approx 1.5$.

The validation experiments involved varying the amount of intralipid and dye by factors of two. If both the dye and scattering concentrations are increased/decreased by the same factor of two, then the measured diffuse reflectance R_d shows only a small change. The results are shown in Fig. 3. The sequences of modulated images (a)–(c) are captured for each of the following three setups:

(a) Blue well: 1× Nigrosin blue, 1× intralipid; Green well: 1× Janus green, 1× intralipid

(b) Blue well: 1× Nigrosin blue, 1× intralipid; Green well: 2× Janus green, 2× intralipid

(c) Blue well: 2× Nigrosin blue, 2× intralipid; Green well: 1× Janus green, 1× intralipid

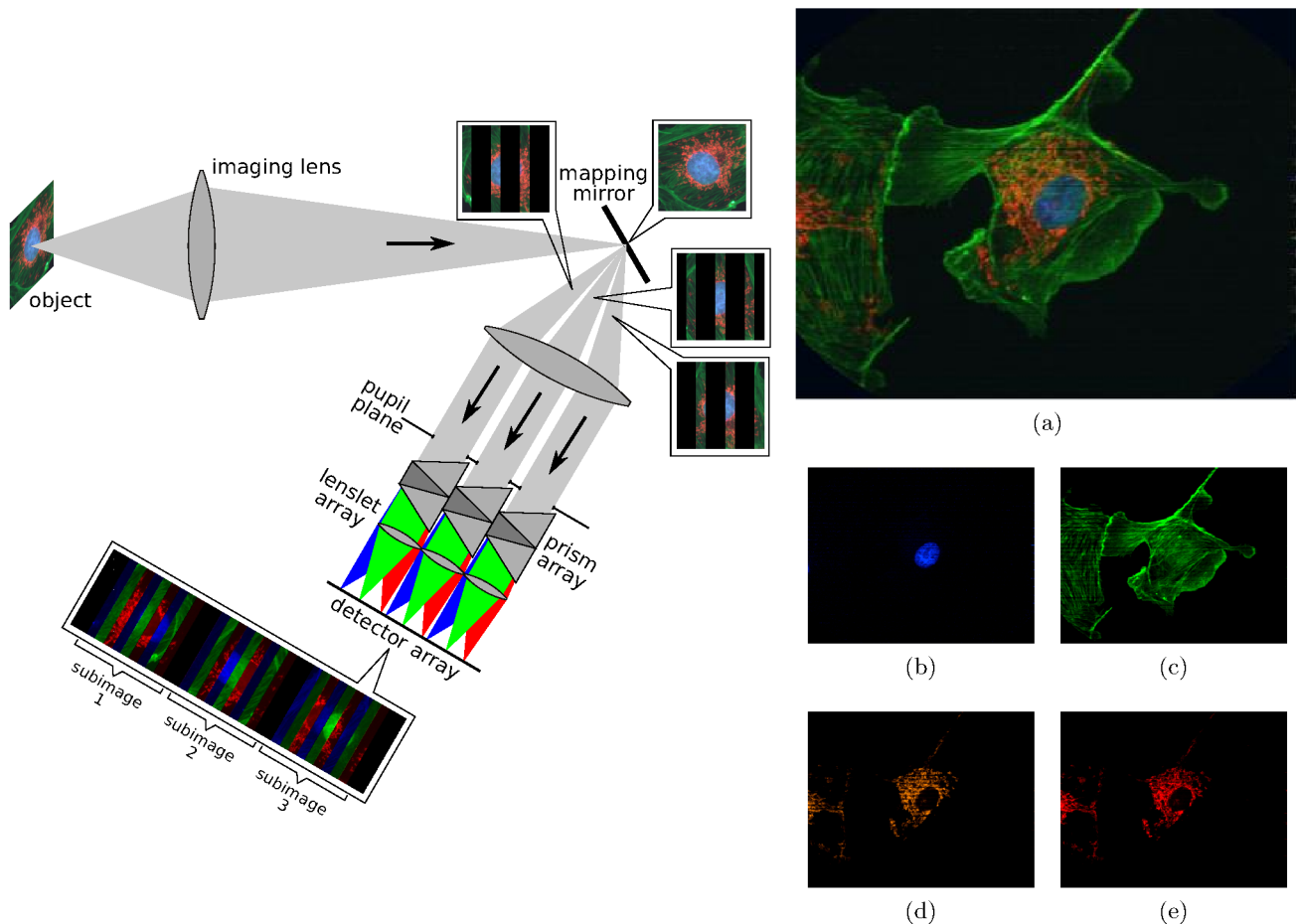(d) Blue well: 2× Nigrosin blue, 2× intralipid; Green well: 2× Janus green, 2× intralipid

Figure 2: (*Left*) The optical layout of the IMS, illustrating how an image is mapped onto the detector array. For simplicity, only three pupils are shown here, whereas a typical IMS has at least 24, laid out in a 2D pattern. (*Right*) An example datacube from an IMS measurement of cells labelled with fluorescent dye, showing a colorized version of the full $(x \times y \times \lambda) = (254 \times 327 \times 45)$ datacube and four selected (x, y) planes (out of 45) of the datacubes — four wavelengths that are reasonably spaced apart and that contain the majority of the signal collected: (*a*) 463 nm, (*b*) 523 nm, (*c*) 595 nm, and (*d*) 622 nm.

Here each increment of Nigrosin blue dye indicates a 0.50% concentration, and each increment of Janus green a 0.33% concentration. The scattering material in the two wells if given in increments of 0.67% intralipid (*ie* 10% intralipid diluted by a factor of 15 in water solution).

Figure 3 shows the repeatability and accuracy of our experimental setup, limited primarily by our ability to control the concentrations of the intralipid and dyes rather than the measurement instrumentation. The presence of changes in the background scattering coefficient have no apparent affect on our ability to quantify the μ_a, and changes in the absorption coefficient have no apparent effect on our ability to quantify μ'_s.

5. EXPERIMENTS: RAT CORTEX IMAGING

Combining the IMS' spectral measurement capability with SFDI allows us to take dynamic measurements of the intrinsic optical signal of the cortex. This signal is produced by changes in diffuse reflectance due to altered blood oxygenation percentage and to changes in blood volume in response to an external stimulus.

For the experiment, five Sprague-Dawley rats were prepared for thinned skull imaging of the cortex according to our standard protocol. Each rat underwent 2 blocks of 64 trials. During each 15 s trial, 1.5 s of prestimulus data followed by 13.5 s of poststimulus data were collected, with an inter-trial interval of 15 seconds. Stimulus
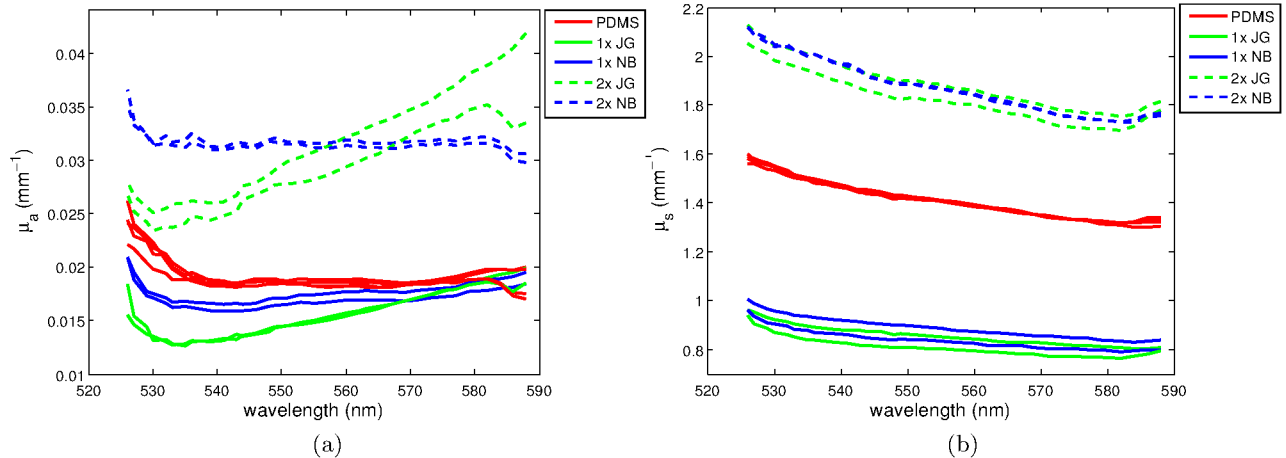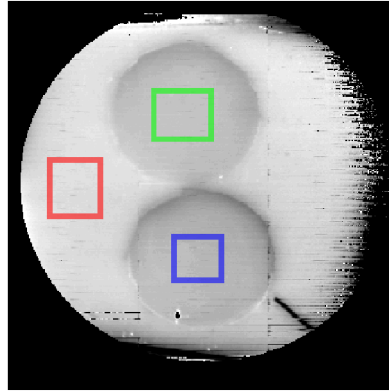
Figure 3: The first validation experiment involves measuring a phantom constructed of silicone (PDMS) with two cylindrical cavities, shown here in diffuse reflectance. (The image contrast has been enhanced in order to make the two cylinders visible.) Two cylindrical cavities are filled with mixtures of diluted intralipid and colored dye — either Nigrosin Blue (NB) or Janus Green (JG) — with varying concentrations. Four separate configurations of concentrations in the wells are shown superimposed. The red, green, and blue boxes shown in the image correspond to the regions of interest over which we average the measured μ_a and μ_s' spectra, shown respectively as red, green, and blue-colored curves in each spectrum plot. (Striped artifacts in the image are due to defects in the mapping mirror used for these experiments.) For exact repeatability, all the curves of a given color/dashing should overlap (for example, the green dashed curves should overlap one another, corresponding to $2\times$ concentration of JG, and the solid blue lines should match one another, corresponding to $1\times$ concentration of NB in different experiment setups.
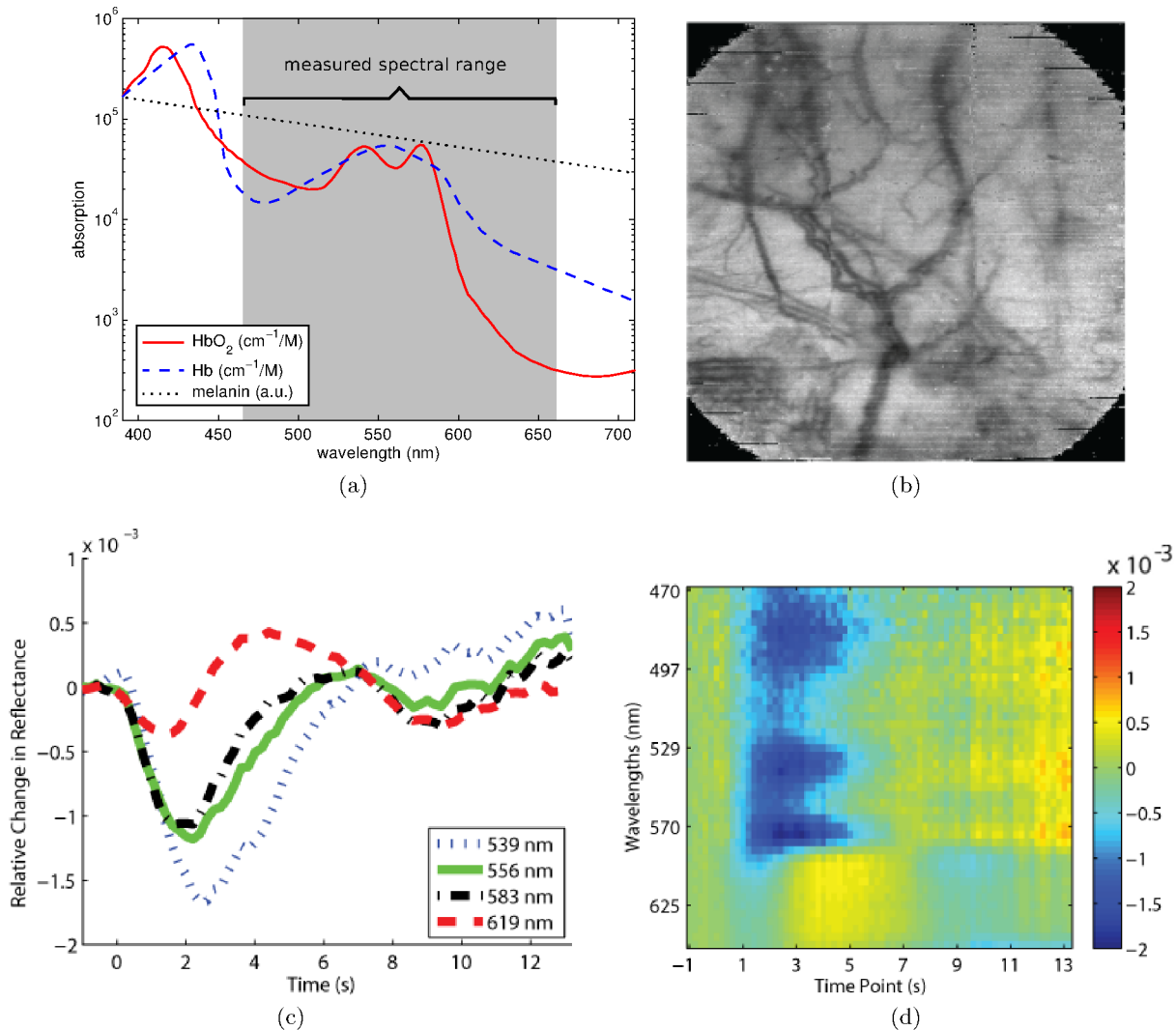
Figure 4: (*a*) Absorption spectra of oxy-/deoxy-hemoglobin (data from Ref. 11) and melanin (data from Ref. 12); (*b*) Example cortex image at 556 nm; (*c*) Relative change in diffuse reflectance ($\Delta R_d/R_d$) during the 15 s experiment for four sample wavelengths; (*d*) The full dataset of $\Delta R_d/R_d$ vs. λ and time from initial stimulus. (Note that the spectral range used here, $470\,nm < \lambda < 660\,nm$ is different from that of the experiments in Section 4.)

consisted of a single whisker (C2) being deflected by 9° in the rostral-caudal direction at a rate of 5 Hz for a total stimulus duration of 1 second. The cortex was illuminated with a tungsten halogen broadband light source and imaged with our existing prototype IMS, which collected images at 46 distinct wavelengths from 470 nm to 650 nm at a rate of 5 Hz. A representative image at 556 nm is shown in Fig. 4(b). Figure 4(c) shows the time course of the relative change in remitted light at the area of peak activation and averaged over a block of 64 trials. Note that most intrinsic signal optical imaging is performed in the 605–630 nm range where the absorption of deoxyhemoglobin is an order of magnitude greater than that of oxyhemoglobin. The curve for 619 nm light reproduces the standard results for intrinsic signal imaging in the rat, including an initial dip before the 2 s mark and an overshoot at the 4 s mark. In Fig. 4(d) the time courses of all 46 wavelengths are represented in false color corresponding to signal intensity and illustrates the sharp change in signal at ~590 nm, where the absorption of oxyhemoglobin drops dramatically. Notice the spectral dips corresponding to the absorption peaks of oxyhemoglobin, and that they are slightly visible during the initial dip, suggesting that an increase in oxyhemoglobin is at least partially responsible for the dip in reflectance measured at 619 nm.

Thus, while our measurements are able to replicate standard data for intrinsic signal imaging of the cortex, they also contain a good deal more due to the IMS' ability to capture a full spectrum at each pixel simultaneously. This can be used both as a check against single-wavelength data and as a means of looking beyond them at other phenomena. We are currently applying a pathlength correction to the above reflectance data in order to directly estimate changes in concentration of oxy- and deoxy-hemoglobin. These are being prepared for a separate publication.

6. CONCLUSION

Snapshot imaging spectrometry provides a high-throughput means of obtaining spectral data using any wide field imaging technique. Here we have adapted an image mapping spectrometer to take data obtained with spatial frequency domain imaging, allowing for rapid quantitative detection of multiple chromophore distributions across tissue. Validation experiments show the robustness of the measurement method (with measurement repeatability limited more by our ability to accurately generate samples of the correct dye and intralipd concentrations). Intrinsic signal optical imaging measurements of the rat cortex show the benefits of using snapshot imaging spectrometry: collecting the entire dataset simultaneously eliminates ambiguities and artifacts caused by scanning, while also providing for both a throughput increase and much faster imaging rate.

REFERENCES

1. D. J. Cuccia, F. Bevilacqua, A. J. Durkin, and B. J. Tromberg, "Modulated imaging: quantitative analysis and tomography of turbid media in the spatial-frequency domain," *Opt. Lett.* **30**, pp. 1354–1356, 2005.
2. D. J. Cuccia, F. Bevilacqua, A. J. Durkin, F. R. Ayers, and B. J. Tromberg, "Quantitation and mapping of tissue optical properties using modulated imaging," *J. Biomed. Opt.* **14**, 024012, 2009.
3. D. Abookasis, C. C. Lay, M. S. Mathews, M. E. Linskey, R. D. Frostig, and B. J. Tromberg, "Imaging cortical absorption, scattering, and hemodynamic response during ischemic stroke using spatially modulated near-infrared illumination," *J. Biomed. Opt.* **14**, 024033, 2009.
4. D. J. Cuccia, D. Abookasis, R. D. Frostig, and B. J. Tromberg, "Quantitative in vivo imaging of tissue absorption, scattering, and hemoglobin concentration in rat cortex using spatially-modulated structured light," in *In Vivo Optical Imaging of Brain Function*, R. D. Frostig, ed., CRC, 2 ed., pp. 339-361, 2009.
5. J. R. Weber, D. J. Cuccia, A. J. Durkin, and B. J. Tromberg, "Noncontact imaging of absorption and scattering in layered tissue using spatially modulated structured light," *J. Applied Physics* **105**, pp. 102028–102036, 2009.
6. A. Mazhar, S. Dell, D. J. Cuccia, S. Gioux, A. J. Durkin, J. V. Frangioni, and B. J. Tromberg, "Wavelength optimization for rapid chromophore mapping using spatial frequency domain imaging," *J. Biomed. Opt.* **15**, 061716, 2010.
7. M. A. A. Neil, R. Juškaitis, and T. Wilson, "Method of obtaining optical sectioning by using structured light in a conventional microscope," *Opt. Lett.* **22**, pp. 1905–1907, 1997.
8. L. Gao, R. T. Kester, and T. S. Tkaczyk, "Compact image slicing spectrometer (ISS) for hyperspectral fluorescence microscopy," *Opt. Express* **17**, pp. 12293–12308, 2009.
9. R. T. Kester, L. Gao, and T. S. Tkaczyk, "Development of image mappers for hyperspectral biomedical imaging applications," *Appl. Opt.* **49**, pp. 1886–1899, 2010.
10. L. Gao, R. T. Kester, N. Hagen, and T. S. Tkaczyk, "Snapshot Image Mapping Spectrometer (ims) with high sampling density for hyperspectral microscopy," *Opt. Express* **18**, pp. 14330–14344, 2010.
11. S. Prahl, "Optical absorption of hemoglobin," accessed Jan 2011.
12. G. Zonios and A. Dimou, "Melanin optical properties provide evidence for chemical and structural disorder *in vivo*," *Opt. Express* **16**, pp. 8263–8268, 2008.